European Polymer Journal 178 (2022) 111486

Contents lists available at ScienceDirect

European Polymer Journal

journal homepage: www.elsevier.com/locate/europolj

pH-sensitive release of antioxidant Se-glycoconjugates through a flexible polymeric patch

Luigia Serpico [a,b,c], Stefania Dello Iacono [a,*], Luca De Stefano [a], Selene De Martino [c], Mario Battisti [c], Principia Dardano [a], Silvana Pedatella [b], Mauro De Nisco [d]

[a] Institute of Applied Sciences and Intelligent Systems, National Research Council, Via P. Castellino 111, Napoli, Italy
[b] Department of Chemical Sciences, University of Napoli Federico II, Via Cintia 4, Napoli, Italy
[c] Materias S.r.l., Corso Nicolangelo Protopisani 50, Napoli, Italy
[d] Department of Sciences, University of Basilicata, Viale dell'Ateneo Lucano 10, Potenza, Italy

ARTICLE INFO

Keywords:
Hydrogels
Selenium glycoconjugates
Antioxidant molecules
Drug delivery
Wound healing
pH-sensitive release

ABSTRACT

In this work, two novel selenium glycoconjugates are proposed as antioxidants to accelerate skin repair. These molecules, designed with more antioxidant sites and improved healing activity, are composed by a selenosugar covalently linked to a caffeic acid or a resveratrol residue. The selenium glycoconjugates have been synthesised and then loaded in a hydrogel flexible film, in order to obtain an active wound dressing. The chemical interaction between the hydrogel and the embedded selenium glycoconjugates can be modulated by the pH values, resulting in a pH-sensitive delivery system. In particular, the caffeic acid-containing compound is released at acute wounds' pH (7.4), while the resveratrol-containing conjugate is released at pH 9.6, typical of chronic wounds. The specific characteristics of the hydrogel and the antioxidant features of the selenium glycoconjugates, as well as the proven controlled release, candidate the designed system at wound care practices.

1. Introduction

Wound care is a widespread health issue and represents a significant cost to the public health system. Wounds are clinically classified in acute and chronic lesions. The formers are temporary and are usually caused by specific factors - like surgery, radiation, chemicals – and they naturally heal in 8–12 weeks. In this kind of wounds, the healing process usually leads to a normal anatomical structure and function restoration of the injured area. On the other hand, chronic wounds represent a persistent status and they are usually related to physio-pathological conditions such as diabetes [1], vascular diseases or prolonged bed rest [2]. Although their prevalence and incidence are difficult to evaluate because of their various management across different regions in the world [3,4], it is estimated that 1–2 % of the population in developed countries will experience a chronic wound during their lifetime [3]. Chronic wounds are characterised by a limited repairing process, in which an optimal anatomical and functional integrity is not reached; this inconvenience usually leads to subsequent complications that require clinical assistance and related financial resources [5]. Several coexisting factors, indeed, can affect the repair, among them the patient age, the presence of vascular, metabolic and autoimmune diseases, as well as an ongoing drug therapy. For these reasons, the incidence of chronic wounds is increased in the elderly population, in which wound closure capacity usually declines [6,7].

Several studies show that Reactive Oxygen Species (ROS) are key regulating factors in skin repair. At low level, ROS are involved in microorganisms killing and promoting the angiogenesis and re-epithelialization, favouring an effective wound closure [8]. By contrast, altered levels of ROS compromise wound's repair. Interestingly, re-establishing the redox balance has been shown to improve the inflammatory skin conditions [9] and restore the healing process, even in chronic wounds, characterised by a persistent oxidative stress [10–13]. Different antioxidant approaches have been investigated to understand their potential beneficial effects in wound repair. With this aim, pharmaceutical and medical companies have proposed and launched on the market a plethora of wearable devices [14] that are more and more patient-friendly, comfortable and smart. In particular, many materials have been investigated and utilised for the fabrication of the so-called "smart patches'', which, rather than only isolating the wound, are also able to actively participate in the wound care process

* Corresponding author.
E-mail address: stefania.delloiacono@cnr.it (S. Dello Iacono).

https://doi.org/10.1016/j.eurpolymj.2022.111486
Received 5 May 2022; Received in revised form 4 August 2022; Accepted 7 August 2022
Available online 10 August 2022

[15], due to the antibacterial [16] or antioxidant substances they contain [17]. Among the explored materials, hydrogels are the most commonly used biomaterials in wound dressing [18]. They, indeed, are flexible, biocompatible and biodegradable, with high potential water content [19]. Hydrogels can crosslink under mild conditions and their biochemical, biophysical and mechanical properties can be tuned as required. In addition, they are water-swollen systems that are able to absorb tissue exudates, promoting tissue regeneration, allowing oxygen to permeate and protecting wounds from microbial invasion [20]. Furthermore, when loaded with bioactive molecules, such as antibiotics, drugs or natural compounds [21], as well as bioactive particles [22] and nanoparticles [23,24], hydrogels can exchange the embedded molecules with the absorbed exudates [25].

Taking into account the avowed advantages of using antioxidants in wound healing [8,26,27] and the wide use of biocompatible hydrogels in wound dressing [28], in this work two glycoconjugates with potential antioxidant activity are tested, and a transdermal delivery system is proposed.

Both the compounds are potential antioxidants since they contain two different active sites in its structure: a selenium atom - inserted in a sugar ring - and a phenolic moiety. It has already been proved, indeed, that a class of selenium compounds, namely selenosugars, are actively involved in skin repair mechanisms [26]. Polyphenols, on the other hand, are a markedly heterogeneous class of natural compounds [29], that have been recognised to have antioxidant effects, beneficial in the prevention of several diseases [30–37] Among polyphenols, the resveratrol shows a series of beneficial biological properties: it can modulate cell proliferation, angiogenesis and redox intracellular equilibrium [38,39]. In a similar way, the caffeic acid has anti-carcinogenic, antimicrobial, anti-inflammatory, antioxidant and immunomodulatory effects both *in vitro* and *in vivo* [40,41]. Because of their promising properties, the resveratrol, as well as the caffeic acid, are widely used in cosmetic and nutraceutical applications.

The exploited hydrogel material is a polymeric blend constituted by two different synthetic polymers, namely poly(hydroxyethyl methacrylate) (HEMA) and poly(ethylene glycol) diacrylate (PEGDA). Hydrogels based on HEMA and PEGDA are largely studied [42] and widely utilised in biomedical applications [43,44], thanks to their non-toxicity and non-immunogenic properties. The Food and Drug Administration (FDA) approves their use for medical purposes, including human intravenous injection, oral and dermal applications [45,46].

The selenium glycoconjugates here proposed are innovative compounds that, with respect to conventional selenosugars, have additional antioxidant sites that could improve their redox activity. In order to exploit the properties of seleno glycoconjugates, a hydrogel-based system has been designed to deliver these compounds in a controlled manner. This polymeric matrix embedding selenium glycoconjugates could be a novel biocompatible dressing to skin repair able to remove ROS from wound site. In addition, this system allows a pH sensitive transdermal delivery of the loaded molecules, due to the specific interaction between each compound and the polymeric material.

2. Material and methods

2.1. General information

All the reagents are acquired (Aldrich, Fluka, Sigma) at the highest purity available and used without further purification. The ^{1}H- and ^{13}C NMR spectra are recorded at 500 and 125 MHz, respectively, on a Fourier Transform NMR Varian 500 Unity Inova spectrometer, or at 400 and 100 MHz, respectively, when a Bruker DRX 400 MHz spectrometer is utilised. $CDCl_3$ is used as a solvent, unless otherwise specified. The proton couplings are evidenced by ^{1}H–^{1}H COSY experiments. The heteronuclear chemical shift correlations are determined by HMQC and HMBC pulse sequences.

2.2. Synthesis of organoselenium compounds

Compounds are prepared according to an already published procedure [47]. The synthetic route provided the chemical conversion of D-ribose **1** into a useful scaffold, the selenosugar **3**. The synthesised compounds are characterised by NMR spectroscopy.

4-((E)-3-acetoxy-5-(((3aR,4S,6aS)-2,2-dimethyltetrahydroselenopheno[3,4–d] [1,3] dioxol-4-yl) methoxy)styryl)phenyl acetate (below called **4**): to a magnetically stirred solution of triphenylphosphine (PPh_3, 393 mg; 1.5 mmol) in anhydrous tetrahydrofuran (2.3 mL) at 0 °C, diisopropyl azodicarboxylate - DIAD (0.303 mL; 1.5 mmol) is added, under N_2. After 15 min a solution of seleno L-sugar **3** (238 mg; 1.0 mmol) and di-acetylated resveratrol (465 mg; 1.5 mmol) in anhydrous tetrahydrofuran - THF (3.0 mL) is added dropwise. The reaction mixture is stirred at room temperature for 3 days. The solvent is evaporated under reduced pressure and replaced with ethyl acetate. The organic layer is washed with a saturated NaCl aqueous solution, dried over anhydrous Na_2SO_4 and filtered. The evaporation of the solvent under reduced pressure gives a crude residue that is purified by silica gel column chromatography (*n*-hexane/diethyl ether) to afford the pure D-sugar derivative **4** (26 % yield). ^{1}H NMR spectrum is reported in S1.

^{1}H NMR (400 MHz): δ 1.36 (s, 3H, CH_3), 1.57 (s, 3H, CH_3), 2.32 (s, 3H, CH_3), 2.33 (s, 3H, CH_3), 3.09 (dd, $J_{1b\text{-}1a}$ = 12.0 Hz, $J_{1b\text{-}2}$ = 1.9 Hz, 1H, H1b), 3.35 (dd, $J_{1a\text{-}1b}$ = 12.0 Hz, $J_{1a\text{-}2}$ = 5.0 Hz, 1H, H1a), 3.86 (ddt, $J_{4\text{-}5b}$ = 8.0 Hz, $J_{4\text{-}5b}$ = 5.2 Hz, $J_{4\text{-}3}$ = 1.8 Hz, 1H, H4), 4.06 (dd, $J_{5b\text{-}5a}$ = 9.7 Hz, $J_{5b\text{-}4}$ = 8.0 Hz, 1H, H5b), 4.24 (dd, $J_{5a\text{-}5b}$ = 9.7 Hz, $J_{5a\text{-}4}$ = 5.2 Hz, 1H, H5a), 4.91 (dd, $J_{3\text{-}2}$ = 5.6 Hz, $J_{3\text{-}4}$ = 1.8 Hz, 1H, H3), 5.06 (ddd, $J_{2\text{-}3}$ = 5.6 Hz, $J_{2\text{-}1a}$ = 5.0 Hz, $J_{2\text{-}1b}$ = 1.9 Hz, 1H, H2), 6.58 (t, J = 1.6 Hz, 1H), 6.88 (t, *J* = 1.9 Hz, 1H), 6.91 (t, J = 1.9 Hz, 1H), 7.00 (d, $J_{7'\text{-}8'}$= 10.9 Hz, 1H, H7′), 7.1 (d, $J_{8'\text{-}7'}$= 10.9 Hz, 1H, H8′), 7.12 (d, J_{orto} = 8.6 Hz, 2H), 7.51 (d, J_{orto} = 8.6 Hz, 2H).

^{13}C NMR (100 MHz): δ 169.4, 159.3, 151.8, 150.3, 139.6, 134.6, 129.1, 127.8, 127.6, 121.9, 112.5, 110.6, 110.3, 107.5, 87.6, 85.2, 70.6, 46.9, 30.3, 26.7, 24.7, 21.1.

3-(((3aR,4S,6aS)-2,2-dimethyltetrahydroselenopheno[3,4–d] [1,3] dioxol-4-yl)methoxy)-5-((E)-4-hydroxystyryl)phenyl acetate (below called **5**): to a magnetically stirred solution of **4** (0.350 g; 0.600 mmol) in THF/methanol 1:1 (1.9 mL), ammonium acetate (0.342 g; 4.44 mmol) is added. The reaction mixture is stirred at room temperature for 2 days. The solvent is evaporated under reduced pressure and replaced with ethyl acetate. The organic layer is washed with a saturated NaCl aqueous solution, dried over anhydrous Na_2SO_4 and filtered. The evaporation of the solvent under reduced pressure gives a crude residue that is purified by silica gel column chromatography (*n*-hexane/ethyl acetate) to afford the pure compound **5** in 53 % yield (0.237 g). ^{1}H NMR spectrum is shown in S2.

^{1}H NMR (500 MHz): δ 1.37 (s, 3H, CH_3), 1.58 (s, 3H, CH_3), 3.09 (dd, $J_{1b\text{-}1a}$ = 11.9 Hz, $J_{1b\text{-}2}$ = 1.5 Hz, 1H, H1b), 3.36 (dd, $J_{1a\text{-}1b}$ = 11.9 Hz, $J_{1a\text{-}2}$ = 5.0 Hz, 1H, H1a), 3.86 (ddt, $J_{4\text{-}5b}$ = 8.1 Hz, $J_{4\text{-}5b}$ = 5.2 Hz, $J_{4\text{-}3}$ = 1.9 Hz, 1H, H4), 4.05 (dd, $J_{5b\text{-}5a}$ = 9.3 Hz, $J_{5b\text{-}4}$ = 8.0 Hz, 1H, H5b), 4.24 (dd, $J_{5a\text{-}5b}$ = 9.3 Hz, $J_{5a\text{-}4}$ = 5.2 Hz, 1H, H5a), 4.92 (dd, $J_{3\text{-}2}$ = 5.5 Hz, $J_{3\text{-}4}$ = 1.3 Hz, 1H, H3), 5.07 (m, 1H, H2), 6.32 (bs, 1H), 6.60 (bs, 1H), 6.61 (bs, 1H), 6.89–6.82 (m, 3H, H7′, H_{orto}), 7.00 (d, $J_{8'\text{-}7'}$= 16.2 Hz, 1H, H8′), 7.40 (d, J_{orto} = 8.5 Hz, 2H).

^{13}C NMR (125 MHz): δ 159.8, 154.0, 141.6, 132.1, 129.9, 128.1, 128.0, 126.0, 115.7, 109.8, 106.3, 105.2, 101.3, 87.7, 85.2, 70.5, 47.1, 30.9, 26.7, 24.7.

(2S,3R,4S)-2-((3-hydroxy-5-((E)-4-hydroxystyryl)phenoxy) methyl)tetrahydro-selenophene-3,4-diol (below called **6**): to the glycoconjugate **5** (2.15 g; 1.0 mmol) a solution (3.3 mL) of acetic acid/H_2O (8:2) is added. The mixture is stirred at 80 °C for 2 h. Then, the solvent is evaporated under reduced pressure and next the organic layer is washed with diethyl ether. The crude residue is purified by preparative thin chromatography (*n*-hexane/ethyl acetate), affording as amorphous solid the pure deprotected product **7** (195.5 mg) with 48 % yield. ^{1}H NMR spectrum is available in supporting information (S3).

^{1}H NMR (500 MHz, acetoneD6): δ 2.86 (dd, $J_{1b\text{-}1a}$ = 10.0 Hz, $J_{1b\text{-}2}$ = 5.2 Hz, 1H, H1b), 3.07 (dd, $J_{1a\text{-}1b}$ = 10.0 Hz, $J_{1a\text{-}2}$ = 5.0 Hz, 1H, H1a), 3.84 (m, 1H, H4), 4.10 (dd, $J_{5b\text{-}5a}$ = 9.6 Hz, $J_{5b\text{-}4}$ = 8.3 Hz, 1H, H5b), 4.15 (m, 1H, H3), 4.50–4.40 (m, 2H, H5b, H2), 6.35 (bs, 1H), 6.35 (t, J_{meta} = 2.1 Hz, 1H), 6.66 (bs, 1H), 6.69 (bs, 1H), 6.86 (d, J_{orto} = 8.5 Hz, 2H), 6.96 (d, $J_{7'\text{-}8'}$ = 16.3 Hz, 1H, H7), 7.13 (d, $J_{8'\text{-}7'}$ = 16.3 Hz, 1H, H8′), 7.46 (d, J_{orto} = 8.5 Hz, 2H).

^{13}C NMR (125 MHz, acetoneD6): δ 160.21, 158.78, 157.4, 140.1, 129.0, 128.7, 127.9, 125.7, 115.5, 106.3, 103.7, 101.1, 78.4, 76.0, 71.5, 42.4, 24.1.

2.3. DPPH test

The radical scavenging activity of compounds towards the radical 2,2-diphenyl-1-picrylhydrazyl (DPPH) is measured as described [48]. Stock solutions of each compound and standard are prepared in ethanol at a concentration of 4 mM (10 mL). Dissolutions (400 – 3.1 μM) are prepared with serial dilutions from stock solutions. After, Tris-HCl 0.1 M (800 μL), each dissolution (200 μL), and DPPH (1 mL) in ethanol (0.2 mM), resulting in a final concentration of 0.1 mM DPPH, are added in glass tubes. Furthermore, a solution with 200 μL of ethanol instead of a sample is prepared. A solution of 800 μL of Tris-HCl buffer and 1.2 mL of ethanol is used as the blank. The mixtures are kept for 30 min at room temperature in the dark, then the absorbance is measured at 517 nm. Ascorbic acid is used as a standard antioxidant. Analysis is done in triplet.

2.4. FRAP assay

The FRAP (ferric reducing/antioxidant power) solution is prepared in acetate buffer (pH 3.6). Stock solutions of each compound and standard are prepared in water at a concentration of 4 mM (10 mL). Dissolutions (400 – 3.1 μM) are prepared with serial dilutions from stock solutions. After, distilled water (1 mL), each dissolution (100 μL), and FRAP solution (1 mL) are added in glass tubes at 37 °C. A solution of 1.1 mL of distilled water and 1 mL of buffer acetate is used as the blank. The mixtures are kept for 7 min at 37 °C and then the absorbance is measured at 593 nm. Ascorbic acid is used as standard. Analysis is done in triplet.

2.5. Patch fabrication

Freestanding PEGDA and PEGDA-HEMA films are prepared mixing a prepolymeric mixture and crosslinking by free radical UV photopolymerization. The HEMA monomer is mixed with PEGDA (Mw 575 Da) at a molar ratio of 4.2:1 (1:1 v/v%). The mixture (50 mL) is magnetically stirred at room temperature for about 10 min, then the photoinitiator (PI) Darocur 1173 (1 % v/v) is added and the mixture is stirred for further 5 min. Then, 60 μL of the resulting solution is placed on a coverslip (15 mm × 15 mm) and covered upside with another glass. The system is exposed for 2 min to UVA light (UVA exposure box, UV-Belichtungsgerät 2), resulting in a crosslinked polymer membrane of about 250 μm thick. The obtained patch is immersed in a solution of Milli-Q (MQ) water (30 mL) for 2 days, at 100 °C to allow the removal of non-crosslinked prepolymer residues and the excess of PI. The membranes are dried overnight at 70 °C.

2.6. Thermal characterization

Thermal gravimetric analysis (TGA) is carried out in dry nitrogen (flow rate of 10 mL/min), using a TA Instrument Q5000. The mass-loss is determined in the scanning mode from 35 to 800 °C with the heating rate of 10 °C/min. Thermal characterization of dry polymer films is performed using TA Instrument Trios differential scanning calorimeter (DSC). Polymer samples, weighing approximately 5 mg, are sealed in TA zero aluminium hermetic pans. Three consecutive temperature-controlled ramps are carried out in N_2 purge (rate of 50 mL/min) to determine thermal transitions: the films are cooled to −60 °C from ambient and equilibrate. The samples are first heated to 180 °C, then cooled to −60 °C and finally again heated to 180 °C: the scanning speed is 10 °C/min in both heating and cooling ramps. TA TRIOS software is used to analyse the DSC traces.

2.7. Fourier transform infrared (FT-IR) spectroscopy

Attenuated total reflection Fourier transform infrared (ATR-IR) spectra are recorded with a Perkin Elmer Frontier FTIR spectrometer with a single reflection universal ATR-IR accessory. A diamond crystal with the angle of incidence for the IR beam of 45° is used. The resolution of the IR spectrum is 4 cm^{-1}; the average is obtained for each sample collecting 32 scans in the wavelength range from 4000 to 650 cm^{-1}.

2.8. Nanoindentation test

Nanoindentation tests are performed using a NanoTest platform (produced by Micro Materials ltd), that monitors the dynamic load and displacement of a three-sided pyramidal diamond indenter Berkovich tip with a radius of about 100 nm. Nanoindentation tests are carried out in load controlled mode in the 0.03–1.00 mN range. For each of 10 measurements, the loading and unloading curves are recorded with a speed of 1.00 mN/s. Depths are in the 5.00 – 15.00 μm range: maximum depth is limited to < 25 μm (10 % of sample thickness) to avoid substrate interference to the measure. The resulting reduced modulus (E_r) is proportional to the slope of the unloading curve where the material recovered its initial condition, and can be related to E via Poisson's ratio (Eq (1)).

$$E_r = \sqrt{\pi} S / 2\beta\sqrt{A} = \left[\left(1-\nu_i^2\right)/E_i + \left(1-\nu_s^2\right)/E_s\right]^{-1} \quad (1)$$

where A is the contact area, β the geometric constant (1.034 for a Berkovich indenter) and S the unloading stiffness at maximum load. E and ν are the elastic modulus and the Poisson's ratio; the subscripts "i" and "s" refer to the diamond indenter and the specimen, respectively. For PEGDA/HEMA copolymer Poisson's ratio is supposed to be 0.35.

2.9. Tensile properties

The elastic modulus and deformation at break of polymer patches are evaluated by means of quasi-static mechanical tests, according to ASTM D-882 standard, performed with a TA-DMA Q800 equipped with tension film clamps. Since the materials are isotropic, seven samples are tested in one direction for each type: the nominal sample sizes are 24.0 × 6.0 × 0.25 mm^3.

The ASTM D-882 standard refers to the tensile testing of thin films (<1 mm), with a width greater than 5 mm and a width-to-thickness ratio greater than 8. The standard recommends testing at least five samples for each material configuration. The Young modulus is evaluated at room temperature in displacement-ramp mode, according to the stress–strain slope up to 2 % strain.

2.10. Atomic force microscopy

A XE-100 Atomic Force Microscopy (AFM) (by Park Systems) is used for the topography reconstruction of loaded and unloaded polymers. Surface imaging is obtained in contact mode at 1 nN using tip C of silicon/aluminium coated NSC36 10 M cantilevers (by Park Systems) 130 μm long with a typical resonance frequency of 65 kHz and nominal force constant of 0.7 N/m. The scan frequency is typically 0.5 Hz per line and the images have 1024x1024 pixels. When necessary, the AFM images have been processed by flattening, in order to remove the background slope, and the contrast and brightness have been adjusted.

2.11. Scanning electron microscopy

Polymeric samples are coated with 15 nm of gold by DC sputtering and imaged by a Field Emission Scanning Electron Microscope (by Carl Zeiss NTS GmbH 1500 Raith FESEM). Images are acquired at 10 kV accelerating voltage with 10 μm wide aperture by InLens detector.

2.12. Swelling ratio (SR)

The swelling properties of the hydrogels are determined by measuring absorption of liquids gravimetrically. The swelling tests are performed at various pH (4.5, 7.4, 8.6 and 9.6), using different buffer solutions. For the swelling tests, the hydrogel specimens are previously dried at 70 °C overnight and weighted, then soaked in buffers with proper pH at 37 °C. At predetermined time intervals, the samples are taken from solution and, after removing the excess surface water with a water-sucking filter paper, their weight is recorded. After each measurement, the hydrogels are immersed again in the buffer solutions until the next weighing. The swelling ratio of the hydrogels is calculated according to Eq (2):

$$SR = [(W_t - W_0)/W_0]^*100 \quad (2)$$

where W_t is the weight of the hydrogel at time t and W_0 is the weight of the dry hydrogel. All swelling ratio values are the average obtained from triplicate samples.

2.13. Antifouling assay

The antifouling properties of investigated materials are evaluated using Bovine serum albumin (BSA). The protein adsorption study is performed using a Bicinchoninic acid (BCA) protein assay. Before testing, a standard calibration curve of BSA is determined (S9). Both samples - PEGDA and PEGDA/HEMA films (15 mm × 15 mm) - are equilibrated in PBS (pH 7.4) for 12 h and then immersed in a BSA solution (2 mg mL^{-1} in PBS) at 37 °C for 24 h. Next, the patches are washed twice with PBS and twice with MQ water. After washing, each film is placed in a well with 1 mL of 2.0 wt% sodium dodecyl sulfonate (SDS) aqueous solution, shaken for 2 h and sonicated for 1 h at room temperature to allow the removal of the absorbed protein on the films. Then, 50 μL of the same SDS solution from each well are added to 1 mL of working reagent solution (according to kit instructions) and the protein concentration is measured by absorbance at 562 nm.

2.14. Drug loading

The patch is immersed in 6 mL of MQ water solution, containing 2.24 mg of compound and the system is kept at 37 °C. The amount of included compound is evaluated by HPLC analysis (Shimadzu SPD-20A) as the difference with respect to the product left in solution. As the glycoconjugate is entered, the patch is dried in oven, at 40 °C overnight. Analysis is done in triplet. Data analysis is executed by excel.

2.15. Compounds' release

Organoselenium compound's release dynamics is performed placing the polymeric membrane in aqueous buffer solutions (10 mL) at different pH (4.5, 7.4, and 9.6). Then, periodically, withdrawals are executed from the release solution and analysed by HPLC (Shimadzu SPD-20A). Release data are reported as the mass percentage of loaded compounds. Analysis is done in triplet. Data analysis is executed by excel.

The controlled release in polymeric systems is described by the Eq (3): [49].

$$\frac{M_t}{M_\infty} = ktn \quad (3)$$

where Mt/M_∞ is the cumulative fractional solute release, t is the release time, k is a constant, and n is the diffusional exponent characteristic of the release mechanism. This general equation can be used to define the release of a solute from a thin polymeric film, regardless of the release mechanism: if $n = 0.5$ solute transport is due to Fickian diffusion; if $n = 1$ it is driven by Case II transport; if $n < 0.5$ or $0.5 < n < 1$ anomalous transport occurs.

Kinetics study in one-dimensional solute release from a thin polymer membrane is carried out solving the Fick's second law of diffusion, with initial and boundary conditions, properly early time (Eq (4)) and late time (Eq (5)) equations: [50,51].

$$\frac{M_t}{M_\infty} \cong 4\left(\frac{D_E}{\pi l^2}\right)^{1/2} \quad (4)$$

$$\frac{M_t}{M_\infty} = 1 - \frac{8}{\pi^2} exp\left(\frac{-\pi^2 D_L t}{l^2}\right) \quad (5)$$

where D_E and D_L are the diffusion coefficients and l is the diffusion distance (half of the film thickness).

3. Results and discussion

In this work, a transdermal delivery system of antioxidant molecules is proposed. The embedded molecules are selenium glycoconjugates - resveratrol containing glycoconjugate - *i.e.*, compound **6** and caffeic acid containing glycoconjugate - *i.e.*, compound **7**. The compound **6** was for the first time reported in this article (Scheme 1) by adapting an already published synthesis [47]. The compound is constituted by a 5 termed selenosugar bound to a resveratrol residue, and its structure was confirmed by NMR analysis. Compound **7** was prepared as reported in Serpico *et al.* [47] and it was constituted by the same selenosugar covalently linked to a caffeic acid moiety. Both the compounds (Fig. 1) showed a good antioxidant activity in different chemical tests (Fig. 2).

3.1. Synthesis

The synthesis of the new glycoconjugate **6** containing two different antioxidant sites, namely a selenium atom and a *trans*-resveratrol residue, was performed. Resveratrol is a phytoalexin present in grape skins and red wine; it possesses different biological activities showing antioxidant, anti-inflammatory and neuroprotective effects. The synthesis was carried out starting from the commercially available D-ribose; selenosugar **3** was obtained and used as glycosyl donor in the following coupling reaction. Then, exploiting the Mitsunobu mechanism, the corresponding glycoconjugate **4** (Scheme 1) was afforded. Next, two following deprotections led to the final product **6**, characterised by mono- and bi-dimensional NMR analysis.

3.2. Antioxidant activity evaluation of synthesised compounds

After synthesis and purification, the new glycoconjugate **6** and the homologue **7** - reported in Fig. 1 - were investigated for their antioxidant properties, consistent with the mechanisms generally accepted for antioxidant compounds.

In order to verify the scavenging and reducing abilities of the compounds, two different chemical antioxidant tests were performed: DPPH and FRAP assays, respectively. In DPPH, the stable free radical showed a characteristic absorption at wavelength 517 nm (Fig. 2a). Noticeably, the typical violet colour of DPPH solution changed when the free radicals were scavenged by antioxidants, becoming yellow. The change of colour, according to the principle of Blois [52], depended on the concentration of radical that was being scavenged, and it could be easily measured and monitored by UV–vis spectroscopy, since the reduction in radical concentration led to a decrease in absorbance. The synthetic glycoconjugates and related precursors were tested at various

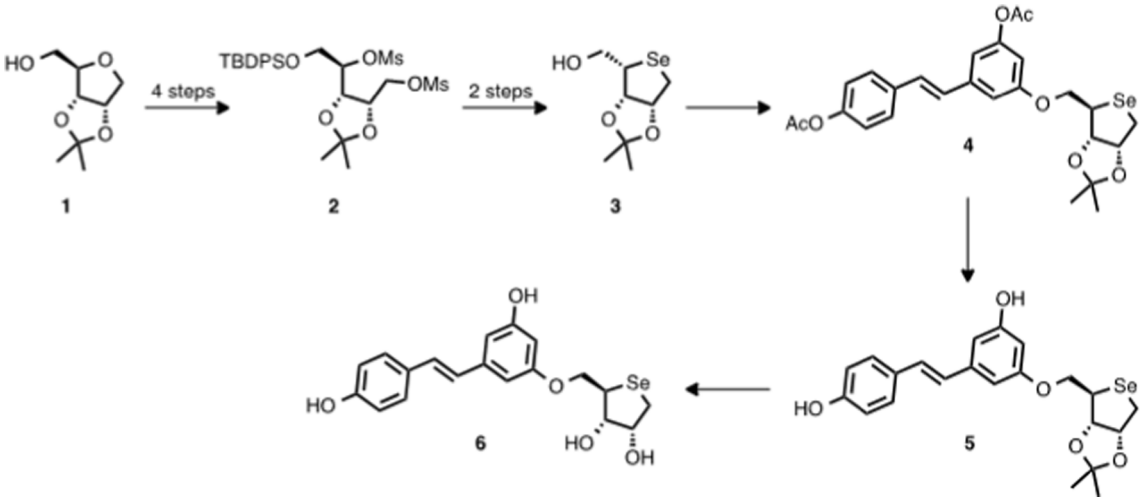

Scheme1. Synthetic route of compound **6**.

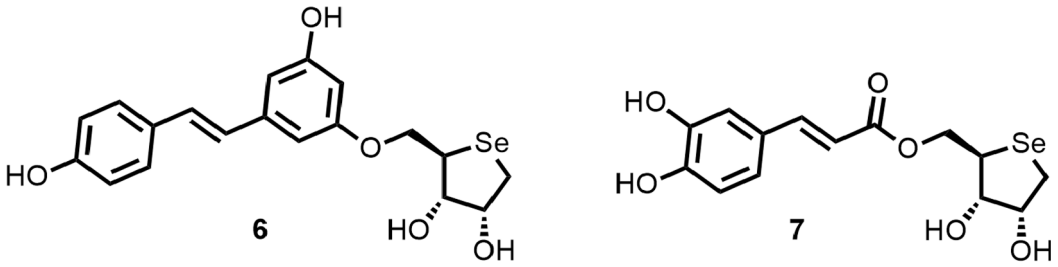

Fig. 1. Resveratrol containing **6** and caffeic acid containing **7** glycoconjugates.

concentrations, within 400 and 3.1 μM.

The FRAP test detected the antioxidant activity of a compound by measuring the increase of the reduced form of the oxidant and the electron flow from reductant to oxidant, in a low pH buffer. In detail, a Fe^{3+} containing complex, $[Fe^{3+}$-(2,4,6-Tris(2-pirydyl)-*s*-triazine$)_2]^{3+}$, was reduced [53] forming $[Fe^{2+}$-(2,4,6-Tris(2-pirydyl)-*s*-triazine$)_2]^{2+}$ and causing the shift of the solution's colour from pale orange to blue (Fig. 2b) [54]. The intensity of the blue colour depended on the amount of Fe^{3+} that was reduced to Fe^{2+} (electron transfer) and it was measured as an increase in the characteristic absorption at 593 nm [55].

For both tests, results were expressed as Efficient Concentration (EC_{50}) values (Fig. 2c). In DPPH, EC_{50} was the concentration of the antioxidant needed to scavenge 50 % of the radicals present in the solution. EC_{50} of FRAP was the concentration of sample or standard that exhibits 50 % of FRAP capacity. The EC_{50} was inversely correlated to the antioxidant capacity of the compound. The lower the EC_{50}, the higher the antioxidant activity of the product [56]. DPPH and FRAP EC_{50} values were compared with the EC_{50} of ascorbic acid (AA), used as reference.

The data showed that both synthetic compounds were good antioxidants for the investigated mechanisms. In detail, the resveratrol containing compound **6** was more active in FRAP, while the caffeic acid glycoconjugate **7** was more effective in the scavenging of radicals. These results were due to the different distribution of –OH active groups on the aromatic structures: compound **6**, indeed, owns two phenolic groups, while compound **7** has a catechol function. The latter oxidised by rapidly transforming into *ortho*-quinone via the proton donation mechanism, resulting more active in DPPH than in FRAP assay. However, compound **7** kept a good activity also in FRAP, in comparison to AA.

3.3. Patch fabrication and characterisation

A thin hydrogel-based membrane was fabricated through photopolymerization of reactive monomers. Reticulation was initiated by a free-radical generating compound, *i.e.* PI, and it was carried out by UV radiation (Fig. 3). In a few minutes, the liquid prepolymeric mixture became solid.

The properties of the thin membrane depended on many factors: the concentration of monomers, the type of blend, the UV radiation time, the amount of PI. With the aim to get the best combination of mechanical and physical properties to allow a suitable delivery of synthesised molecules, polymeric films with different compositions were prepared. In detail, the effect of a partial replacement of PEGDA 575 with HEMA was evaluated: patches consisting of only PEGDA and a blend of PEGDA 575 and HEMA in 1 to 1 v/v% were tested.

The thermal stability was analysed monitoring the degradation by thermogravimetric analysis in dry nitrogen. The TGA curves in S4 showed remarkable thermal stability: the onset of the thermal decomposition of both polymers was observed at temperatures over 150 °C.

The DSC analysis was performed to evaluate the curing degree of prepolymeric mixtures. Thermal analysis of both PEGDA and PEGDA/HEMA 3D hydrogels showed a complete polymerization, without residual crosslinking enthalpy, with glass transition temperatures (*Tg*) at −19 °C and 17 °C, respectively (Fig. 4a).

The FTIR spectra of both unreacted and crosslinked monomers (S5) confirmed the complete polymerization. The peak at 1640 cm^{-1} - typical of C═C stretching vibrations - and the peaks at 810 cm^{-1} and at 1298 cm^{-1}, proper of the vinyl group = CH bending and deformation, respectively, disappear in the spectra of cured polymers, proving the polymeric chains interconnection.

Furthermore, ATR spectra (Fig. 4b) showed the main chemical differences between the 3D polymers. The characteristic broad band at 3400 cm^{-1} corresponded to the O—H stretching vibration of the hydroxyl group; the bands in the range 2945–2875 cm^{-1} were owing to the symmetric and asymmetric stretching vibrations of CH_2 and CH_3 in

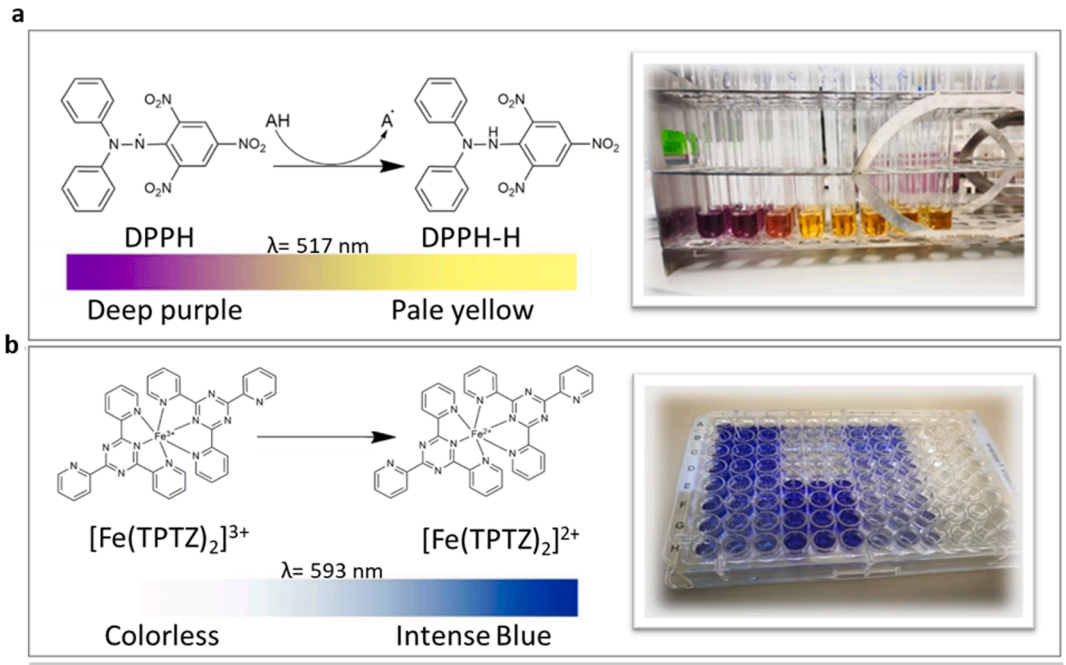

c

COMPOUND	EC_{50} (μM) DPPH	EC_{50} (μM) FRAP
6	36.35±2.72	26.48±3.60
7	9.57±0.67	24.10±1.84
AA	25.59±1.80	24.55±5.34

Fig. 2. Antioxidant tests: **a)** DPPH scavenging assay; **b)** FRAP assay; **c)** EC_{50} values of both compounds **6** and **7** and reference (AA).

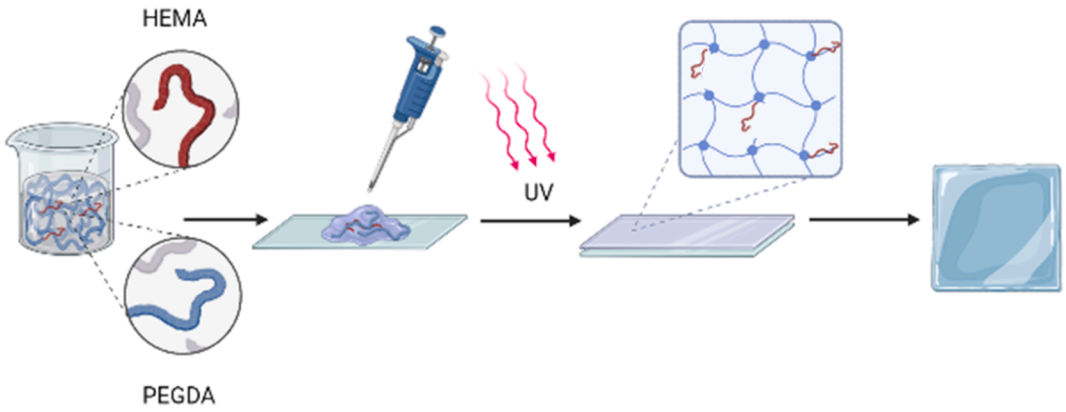

Fig. 3. Fabrication process of polymeric patch (PEGDA 575/HEMA) via photolithography (Figure created with Biorender).

HEMA portion.

The mechanical properties of PEGDA and PEGDA/HEMA patches were evaluated with two different approaches: tensile strength tests performed by a DMA machine and nanoindentation tests. The representative stress–strain curves (Fig. 4c) clearly showed higher strain (Fig. 4d) at fracture (ε_b) and lower elastic modulus (E) value (Fig. 4e) for PEGDA/HEMA specimens compared to PEGDA samples. PEGDA/HEMA exhibited 11.2 ± 1.9 % and 9.8 ± 2.3 MPa, ε_b and E, respectively; while PEGDA had 4.9 ± 0.8 % and 26.6 ± 3.8 MPa, strain at fracture and modulus values. The increase in mechanical tensile properties was attributable to a less densely crosslinked polymer network in PEGDA/HEMA which results in a less rigid structure, compared to PEGDA.

This behaviour was confirmed by the nanoindentation test: Fig. 4f, indeed, showed the reduced modulus (E_r) and hardness (H) for both patches. Reduced modulus for PEGDA/HEMA (13.8 ± 4.4 MPa) was much less than the one of PEGDA (49.2 ± 3.2 MPa). It has to be taken into account that E calculated from E_r, measured by depth sensing indentation, is always 5–20 % higher than the one obtained from tensile test [57]. The hardness, measured as ratio of the maximum load exerted and the effective contact area, was about ten times lower for PEGDA/HEMA (1.0 ± 0.3 MPa) than for PEGDA (9.1 ± 1.2 MPa). Finally, the morphological analysis was carried out performing SEM and AFM characterisation (S6). The morphology and the roughness (PEGDA 1.6 nm, PEGDA/HEMA 1.0 nm) of the surfaces were comparable, not showing significant differences between the samples.

Both macroscopic and microscopic results supported the conclusion that partial replacement of PEGDA with HEMA increased the flexibility of the patch, without detrimental effects on the material thermal

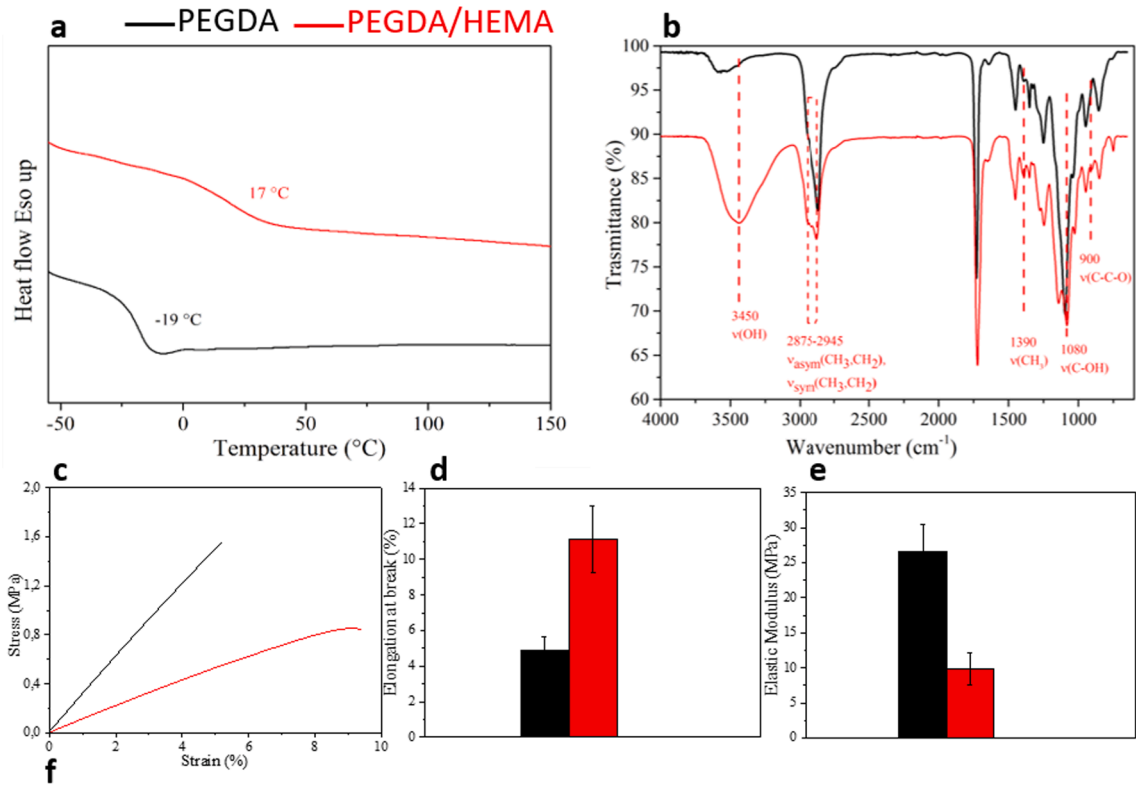

f

Nanoidentation	Reduced Modulus Er [MPa]	Hardness [MPa]
PEGDA	49.18±3.18	9.14±1.15
PEGDA/HEMA	13.79±4.40	1.01±0.26

Fig. 4. Crosslinked PEGDA and PEGDA/HEMA comparison: **a)** T_g values in DSC traces; **b)** ATR-IR spectra; **c)** representative stress–strain curves; **d)** elongation at break values; **e)** elastic moduli; **f)** nanoindentation results.

stability.

3.4. Swelling ratio and antifouling properties

Swelling is one of the main characteristics of hydrogels. It can affect mechanical properties, as well as loading and releasing kinetics of embedded compounds. The effect of HEMA amount on the water uptake capacity of the membranes was evaluated measuring the SR of both PEGDA and PEGDA/HEMA patches. The related results are shown in Fig. 5a as a function of time. Both the polymeric patches reached the swelling equilibrium after 15 min, maintaining a constant weight up to 72 h. It is noteworthy that the blended patch showed a higher swelling capacity, reaching a SR of 38.4 % ± 0.7 in 15 min, instead of the 28.4 % ± 0.6 registered by the PEGDA membrane. As expected, the swelling capacity increased as the crosslinking density decreased, and the affinity with water rose, partially replacing PEGDA with HEMA monomers. The presence of a significant amount of the most hydrophilic component HEMA (molar fraction PEGDA/HEMA ~ 0.24) improved the swelling ability of the system by about 30 % [58].

With the aim to investigate how the pH affects the swelling properties, SR of both polymeric materials at different pH (4.5, 7.4, 8.6 and 9.6) was evaluated. As shown in S7, hydrogel swelling behaviour over time was not uniquely related to pH value. SR, indeed, increased significantly in the first minutes, reached an extreme in 15 min and remained constant for several hours; this dynamic was verified for all the investigated conditions. With the naked eye, both materials retained their shape and self-sustainability, while dimensions expanded isotropically with increasing SR (S8). These characteristics make both patches useful in a large pH range, thus in different stages of a wound. If, indeed, in initial/acute phases the pH is around at the physiological value, in chronic wounds the pH increases being included between 7.5 and 10.

In detail, Fig. 5b showed the hydrogel swelling degree ratios at equilibrium (SR_∞) of both patches (PEGDA and PEGDA/HEMA) as a function of pH. Even though the variation was really narrow, it could be observed that PEGDA exhibited the highest SR_∞ at acid pH (4.5) and it slightly decreased at higher pH values. The blended patch, on the other hand, showed the opposite profile: the highest SR_∞, indeed, were measured at pH values included between 7 and 10 which correspond to the wound pHs. Coherently, PEGDA/HEMA blend exhibited a mild reduction of the water uptake value at pH 4.5 (aqueous solution of NaOAc/AcOH), probably due to the presence of the acetic counterion that decreased the solvent power of water. Thus, hydrophilic solvent-polymer interactions, especially due to HEMA monomers, became weaker while hydrophobic ones between polymer chains were favoured. Probably, at basic pH values, the negative charges of the deprotonated hydroxyl groups of HEMA ($-O^-$) caused a repulsive force that, in turn, increased the mesh of the network and, consequently, the swelling grade.

To be noted, the PEGDA/HEMA patch reached the highest SR_∞ at all the investigated pHs and the largest difference in SR_∞ between PEGDA and PEGDA/HEMA was recorded in pH range of interest for the wound

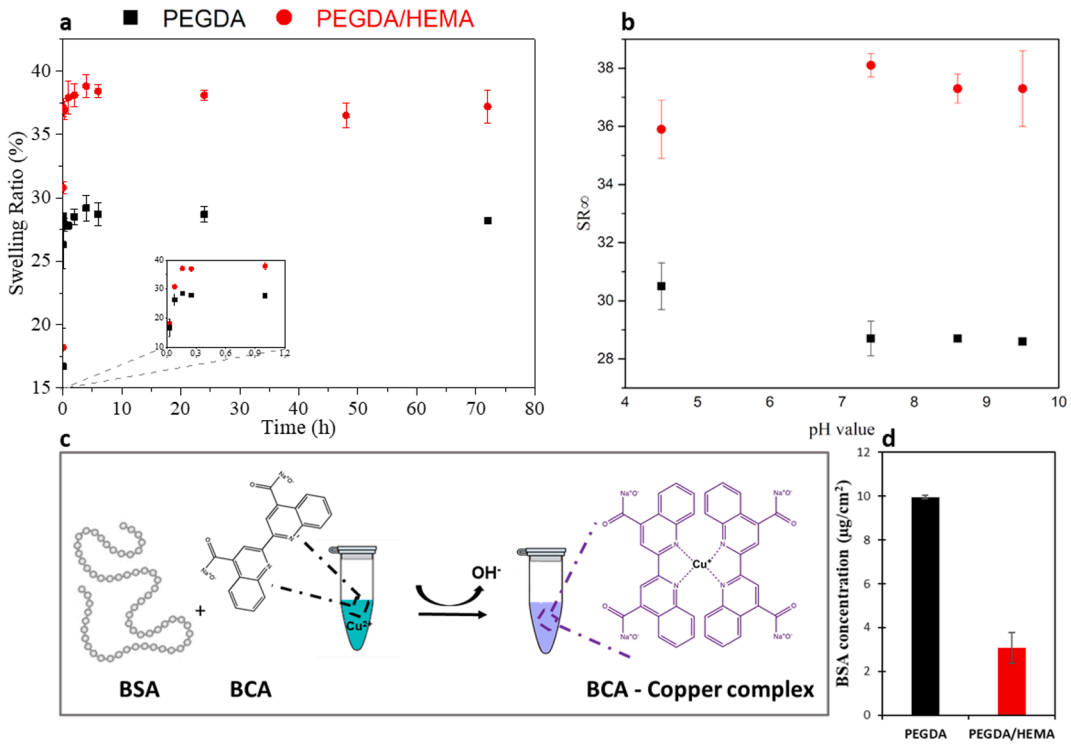

Fig. 5. **a)** Swelling ratio of PEGDA and PEGDA/HEMA patches soaked in MQ water, at 37 °C - in the inset measurements recorded in the first hour are reported; **b)** SR at equilibrium swelling as function of pH values; **c)** antifouling test based on BCA reaction; **d)** BSA concentration detected on both materials.

dressing application, confirming the choice of polymeric blend as fabrication material. Since the system here proposed is potentially intended for wound care, antifouling properties have to be evaluated. Protein adsorption on the material, indeed, could promote microbial coating affecting the healing process. In this work, BSA was chosen as a representative protein, to investigate the protein-resistant ability of both PEGDA and PEGDA/HEMA membranes. The patches were soaked in BSA solution (2 mg mL^{-1}) for 24 h at 37 °C and then, adsorbed protein was quantitatively determined using the BCA assay (Fig. 5c and d). The results showed a low adsorption of BSA on both investigated materials. The recorded values, 10.0 ± 0.1 μg cm^{-2} and 3.1 ± 0.7 μg cm^{-2} for PEGDA and PEGDA/HEMA respectively, demonstrated that the HEMA content improved the non-fouling properties of material. Taking into account the reported advantages of the PEGDA/HEMA patch, only this one has been used for the loading of antioxidant molecules.

3.5. Drug loading and release dynamics

Materials' characterization and analysis of mechanical properties of both fabricated patches showed that the PEGDA/HEMA one has the best properties for the desired purpose, so that it was investigated for the loading and release properties quantification. In detail, the membrane was firstly loaded with each of two compounds **6** and **7** (Fig. 6a) and then a complete characterisation of the final systems was carried out by thermal, mechanical (S10) and morphological analysis (S11).

To investigate the loading capacity of chosen material, the patch was immersed in an ultrapure water solution of each glycoconjugate. The amount of loaded compound was verified with periodic withdrawals from the aqueous loading solution and then analysed by HPLC. Specifically, the maximum loading was reached after 3 days for compound **6** (96 ± 2 %), and after 5 days for compound **7** (63 ± 4 %).

Mechanical and thermal characterizations were performed on the final systems in order to exclude any eventual effect of the molecules on the polymer properties. As expected, no appreciable difference was recorded in thermal stability, T_g value, as well as elongation at break and Young modulus (S10).

SEM images showed that both samples have similar characteristics; moreover, AFM analysis revealed a comparable roughness that was 1.3 nm for patch loaded with compound **6** and 2.8 nm for the one containing compound **7**. These slight differences in the loaded patches suggested that both compounds did not strongly interact with the polymer matrix. Moreover, the mild differences also in the roughness between loaded and unloaded material indicated that both the compounds did not aggregate during the loading procedure. The performed characterisation demonstrated that the compounds' loading did not alter any of the main properties of the polymeric membrane, making them interesting as drug delivery systems.

In order to study the drug delivery capacity of the systems and the role of the pH in dynamics release, the amount of compounds released over time at diverse pH values was recorded. In detail, the loaded patches were immersed in buffered solutions at pH 4.5, 7.4 and 9.6. Interestingly, at pH 4.5 neither compound **6** nor **7** were released. For compound **6**, no release was detected even at pH 7.4, while a significant amount was found at basic conditions. More precisely, at pH 9.6 (Fig. 6b) the dynamics followed a regular and sustained profile: more than 20 % of loaded compound was delivered in the first 10 h, reaching the 25 % in 24 h and ca. 30 % in 72 h.

On the other hand, a not gradual release of **7** was observed at pH 9.6: in the first hour ca. 20 % of the loaded glycoconjugate was detected and this value remained fixed until the 24 h. Conversely, compound **7** showed a sustained delivery at physiological pH, reaching ca. 70 % in 24 h (Fig. 6c).

The diverse dynamics were probably due to the hydrogen bonds and van der Waals interactions that the two compounds, in different pH conditions, could form with disposable groups of polymers, besides the spatial configuration of the glycoconjugates. Probably the related interactions were due to the own pKa value of cathecolic and phenolic functions, exhibiting different protonation degrees at the investigated pH values.

The above mentioned compounds' characteristics may also affect the

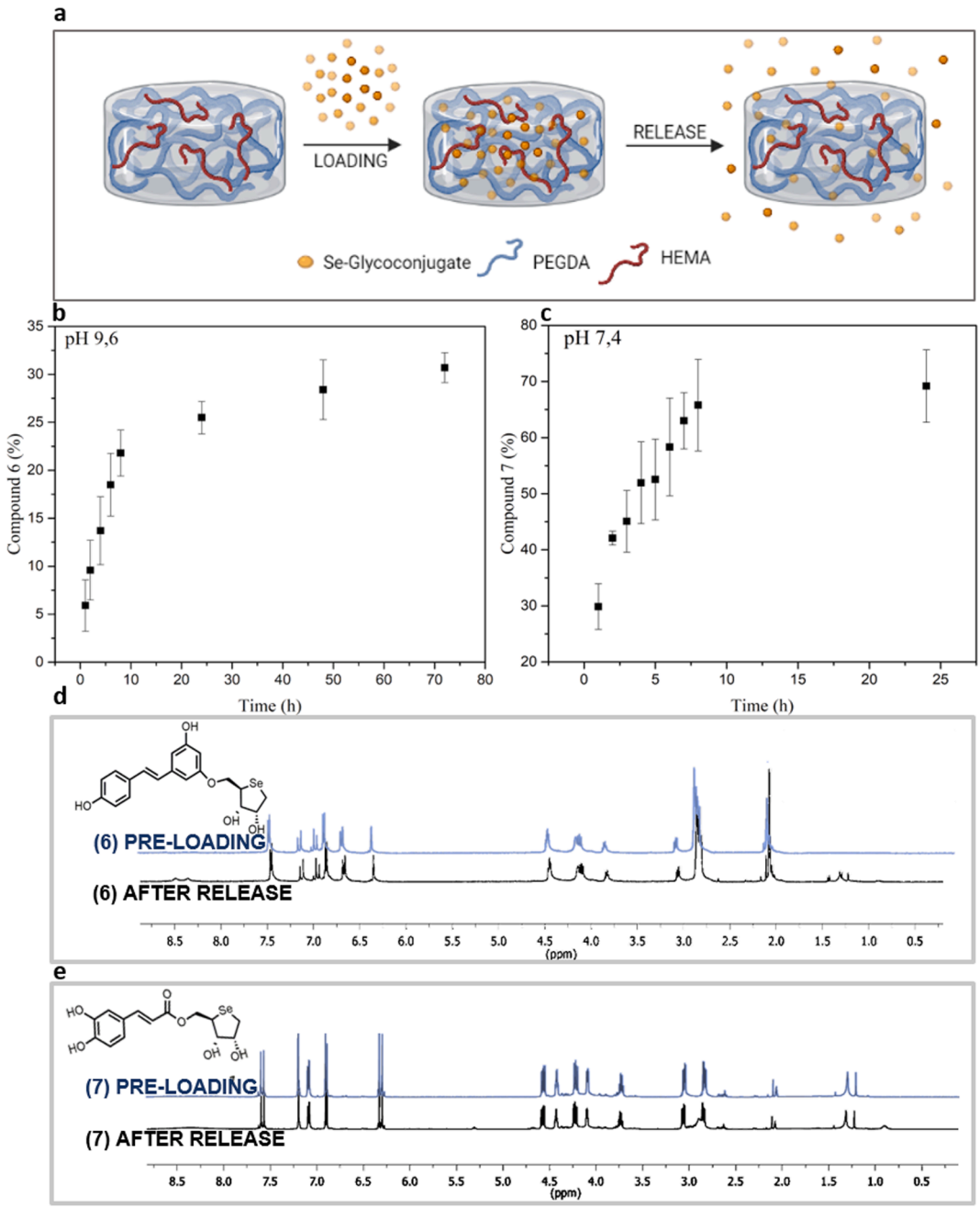

Fig. 6. Loading and release processes: **a)** schematic representation of loading and release process (Figure created with Biorender); **b)** release profile of compound **6** at pH 9.6; **c)** release profile of compound **7** at pH 7.4; **d)** ^{1}H-NMR of compound **6** before the loading and after the release; **e)** ^{1}H-NMR of compound **7** before the loading and after the release.

release order. Numeric analysis of the diffusion coefficients (D) at 40 °C, according to early (D_E) and late (D_L) -time approximations for the release, showed that diffusion coefficients decreased with increasing polymer matrix/compound interaction (S12). In addition, the ultimate cumulative release depended on the chemical structure of the solute, resulting in a lower amount as well as in a slower release for the compound **7** than the compound **6**. The fit analysis based on experimental data, recorded at the selected pH, showed an anomalous transport mechanism for both selenium glycoconjugates: anomalous Case II transport for compound **6** and anomalous Fickian for compound **7** (S12).

After the release, the structural integrity of both compounds was confirmed by NMR study (Fig. 6d-e). As shown, a comparative analysis of ^{1}H NMR of each compound, as synthesised and after the release, confirmed that the molecules were not altered. This evidence was also supported by the HPLC analysis (S13 and S14): chromatograms did not show any additional peak. These results clearly indicated that compounds maintain their activity.

4. Conclusions

Here, a new polymeric system for the delivery of bioactive molecules, potentially involved in skin repair, has been developed. Two selenium glycoconjugates were synthesised and their antioxidant activity was proved. A biocompatible copolymer, consisting of PEGDA and HEMA in molar ratio 1:4.2, was selected as the matrix for the delivery system. The material, as well as the delivery system were characterised, showing suitable thermomechanical properties.

The combination compounds-polymer resulted in pH-sensitive

controlled delivery systems. In particular, each compound is released at a specific pH, paving the way for a selective pH responsive application. The caffeic acid containing conjugate, indeed, is delivered at pH 7.4 - typical of acute injuries - while the resveratrol compound is released at pH 9.6 that corresponds to the pH value of chronic wounds. This pH driven delivery is due to the specific and weak interactions between functional groups of compounds and the –OH functions of HEMA polymer. The suitable characteristics of selected hydrogels and the antioxidant capacity of the synthesised molecules, as well as the proven controlled release, open the possibility to apply the ideated system in wound care practices.

Funding

European Union FSE, PON Ricerca e Innovazione 2014–2020, Azione I.1 "Dottorati Innovativi con caratterizzazione Industriale" provided a PhD grant to Luigia Serpico.

CRediT authorship contribution statement

Luigia Serpico: Investigation, Methodology, Writing – original draft. **Stefania Dello Iacono:** Conceptualization, Investigation, Methodology, Project administration, Supervision, Writing – original draft. **Luca De Stefano:** Conceptualization, Project administration, Supervision. **Selene De Martino:** Investigation, Writing – review & editing. **Mario Battisti:** Investigation, Writing – review & editing. **Principia Dardano:** Writing – review & editing. **Silvana Pedatella:** Methodology, Investigation, Writing – review & editing. **Mauro De Nisco:** Investigation, Methodology.

Declaration of Competing Interest

The authors declare the following financial interests/personal relationships which may be considered as potential competing interests: [Stefania Dello Iacono has patent #102021000012806 pending to Avicenna Natural Institute Srl. Luigia Serpico has patent #102021000012806 pending to Avicenna Natural Institute Srl. Silvana Pedatella has patent #102021000012806 pending to Avicenna Natural Institute Srl. Mauro De Nisco has patent #102021000012806 pending to Avicenna Natural Institute Srl. Luca De Stefano has patent #102021000012806 pending to Avicenna Natural Institute Srl.].

Data availability

Data will be made available on request.

Acknowledgement

The authors would like to thank Mr. Mario De Angioletti (CNR-IPCB) and Ms. Maria Rosaria Marcedula (CNR-IPCB) for the useful support in nanoindentation and DSC tests, respectively; Avicenna Natural Institute S.r.l. as industrial partner of "Dottorati Innovativi con caratterizzazione Industriale" project.

Data availability

The raw/processed data required to reproduce these findings cannot be shared at this time as the data also forms part of an ongoing study.

Appendix A. Supplementary material

Supplementary data to this article can be found online at https://doi.org/10.1016/j.eurpolymj.2022.111486.

References

[1] J.H. Kim, B. Yang, A. Tedesco, E.G.D. Lebig, P.M. Ruegger, K. Xu, J. Borneman, M. Martins-Green, High levels of oxidative stress and skin microbiome are critical for initiation and development of chronic wounds in diabetic mice, Sci. Rep. 9 (2019) 19318.
[2] A. Moeini, P. Pedram, P. Makvandi, M. Malinconico, G. Gomez d'Ayala, Wound healing and antimicrobial effect of active secondary metabolites in chitosan-based wound dressings: A review, Carbohydr. Polym. 233 (2020) 115839.
[3] K. Järbrink, G. Ni, H. Sönnergren, A. Schmidtchen, C. Pang, R. Bajpai, J. Car, Prevalence and incidence of chronic wounds and related complications: a protocol for a systematic review, Syst. Rev. 5 (2016) 152.
[4] L. Martinengo, M. Olsson, R. Bajpai, M. Soljak, Z. Upton, A. Schmidtchen, J. Car, K. Järbrink, Prevalence of chronic wounds in the general population: systematic review and meta-analysis of observational studies, Ann. Epidemiol. 29 (2019) 8–15.
[5] G. Han, R. Ceilley, Chronic wound healing: a review of current management and treatments, Adv. Ther. 34 (2017) 599–610.
[6] M.J. Blair, J.D. Jones, A.E. Woessner, K.P. Quinn, Skin structure-function relationships and the wound healing response to intrinsic aging, Adv. Wound Care. 9 (3) (2020) 127–143.
[7] Z. Doozandeh, S. Saber-Samandari, A. Khandan, Preparation of novel arabic Gum-C6H9NO biopolymer as a bedsore for wound care application, Acta Med. Iran. (2020) 520–530.
[8] M. Cano Sanchez, S. Lancel, E. Boulanger, R. Neviere, Targeting oxidative stress and mitochondrial dysfunction in the treatment of impaired wound healing a systematic review, Antioxidants (Basel) 7 (8) (2018) 98.
[9] C. Dunnill, T. Patton, J. Brennan, J. Barrett, M. Dryden, J. Cooke, D. Leaper, N. T. Georgopoulos, Reactive oxygen species (ROS) and wound healing: the functional role of ROS and emerging ROS-modulating technologies for augmentation of the healing process, Int. Wound J. 14 (2017) 89–96.
[10] J.-D. Luo, Y.-Y. Wang, W.-L. Fu, J. Wu, A.F. Chen, Gene therapy of endothelial nitric oxide synthase and manganese superoxide dismutase restores delayed wound healing in type 1 diabetic mice, Circulation 110 (16) (2004) 2484–2493.
[11] G.P. Fadini, M. Albiero, L. Menegazzo, E. Boscaro, E. Pagnin, E. Iori, C. Cosma, A. Lapolla, V. Pengo, M. Stendardo, C. Agostini, P.G. Pelicci, M. Giorgio, A. Avogaro, The redox enzyme p66Shc contributes to diabetes and ischemia-induced delay in cutaneous wound healing, Diabetes 59 (2010) 2306–2314.
[12] A.L. Weinstein, F.D. Lalezarzadeh, M.A. Soares, P.B. Saadeh, D.J. Ceradini, Normalizing dysfunctional purine metabolism accelerates diabetic wound healing, Wound Repair Regen. 23 (1) (2015) 14–21.
[13] S. Tao, R. Justiniano, D.D. Zhang, G.T. Wondrak, The Nrf2-inducers tanshinone I and dihydrotanshinone protect human skin cells and reconstructed human skin against solar simulated UV, Redox Biol. 1 (1) (2013) 532–541.
[14] A. Farazin, Z. Torkpour, S. Dehghani, R. Mohammadi, M.D. Fahmy, S. Saber-Samandari, K. Adel Labib, A. Khandan, A review on polymeric wound dress for the treatment of burns and diabetic wounds, Int. J. Basic Sci. Med. 6 (2021) 44–50.
[15] C. Cui, S. Sun, S. Wu, S. Chen, J. Ma, F. Zhou, Electrospun chitosan nanofibers for wound healing application, Eng. Regener. 2 (2021) 82–90.
[16] F.S. Abadehie, A.H. Dehkordi, M. Zafari, M. Bagheri, S. Yousefiasl, S. Pourmotabed, L. Mahmoodnia, M. Validi, M. Ashrafizadeh, E.N. Zare, N. Rabiee, P. Makvandi, E. Sharifi, Lawsone-encapsulated chitosan/polyethylene oxide nanofibrous mat as a potential antibacterial biobased wound dressing, Eng. Regener. 2 (2021) 219–226.
[17] X. Zhao, H. Wu, B. Guo, R. Dong, Y. Qiu, P.X. Ma, Antibacterial anti-oxidant electroactive injectable hydrogel as self-healing wound dressing with hemostasis and adhesiveness for cutaneous wound healing, Biomaterials 122 (2017) 34–47.
[18] S. Wu, L. Deng, H. Hsia, K. Xu, Y.u. He, Q. Huang, Y.i. Peng, Z. Zhou, C. Peng, Evaluation of gelatin-hyaluronic acid composite hydrogels for accelerating wound healing, J. Biomater. Appl. 31 (10) (2017) 1380–1390.
[19] E. Lih, J.S. Lee, K.M. Park, K.D. Park, Rapidly curable chitosan-PEG hydrogels as tissue adhesives for hemostasis and wound healing, Acta Biomater. 8 (9) (2012) 3261–3269.
[20] I. Harrison, F. Spada, Hydrogels for atopic dermatitis and wound management: a superior drug delivery vehicle, Pharmaceutics. 10 (2) (2018) 71.
[21] C. Gong, Q. Wu, Y. Wang, D. Zhang, F. Luo, X. Zhao, Y. Wei, Z. Qian, A biodegradable hydrogel system containing curcumin encapsulated in micelles for cutaneous wound healing, Biomaterials 34 (27) (2013) 6377–6387.
[22] Y. Hou, J. Li, S. Guan, F. Witte, The therapeutic potential of MSC-EVs as a bioactive material for wound healing, Engineered Regeneration. 2 (2021) 182–194.
[23] H. Liang, M.S. Mirinejad, A. Asefnejad, H. Baharifar, X. Li, S. Saber-Samandari, D. Toghraie, A. Khandan, Fabrication of a review on nthin gum-carboxymethyl chitosan bio-nanocomposite wound dressing with silver-titanium nanoparticles using freeze-drying method, Mater. Chem. Phys. 279 (2022), 125770.
[24] A. Raisi, A. Asefnejad, M. Shahali, Z. Doozandeh, B. Kamyab Moghadas, S. Saber-Samandari, A. Khandan, A soft tissue fabricated using a freeze-drying technique with carboxymethyl chitosan and nanoparticles for promoting effects on wound healing, J. Nanoanal. 7 (2020) 262–274.
[25] J. Xiang, L. Shen, Y. Hong, Status and future scope of hydrogels in wound healing: Synthesis, materials and evaluation, Eur. Polym. J. 130 (2020), 109609.
[26] M.J. Davies, C.H. Schiesser, 1,4-Anhydro-4-seleno-d-talitol (SeTal): a remarkable selenium-containing therapeutic molecule, New J. Chem. 43 (2019) 9759–9765, https://doi.org/10.1039/c9nj02185j.
[27] Z. Ahmadian, A. Correia, M. Hasany, P. Figueiredo, F. Dobakhti, M.R. Eskandari, S. H. Hosseini, R. Abiri, S. Khorshid, J. Hirvonen, H.A. Santos, M.-A. Shahbazi, A hydrogen-bonded extracellular matrix-mimicking bactericidal hydrogel with

radical scavenging and hemostatic function for pH-responsive wound healing acceleration, Adv. Healthc. Mater. 10 (3) (2021) 2001122.
[28] Z. Xu, S. Han, Z. Gu, J. Wu, Advances and impact of antioxidant hydrogel in chronic wound healing, Adv. Healthc. Mater. 9 (5) (2020) 1901502.
[29] C.S. Cutrim, M.A.S. Cortez, A review on polyphenols: Classification, beneficial effects and their application in dairy products, Int. J. Dairy Technol. 71 (2018) 564–578.
[30] A.M. Mileo, P. Nisticò, S. Miccadei, Polyphenols: immunomodulatory and therapeutic implication in colorectal cancer, Front. Immunol. 10 (2019) 729.
[31] A. Thyagarajan, A.S. Forino, R.L. Konger, R.P. Sahu, Dietary polyphenols in cancer chemoprevention: implications in pancreatic cancer, Antioxidants (Basel). 9 (8) (2020) 651.
[32] S. Sajadimajd, R. Bahramsoltani, A. Iranpanah, J. Kumar Patra, G. Das, S. Gouda, R. Rahimi, E. Rezaeiamiri, H. Cao, F. Giampieri, M. Battino, R. Tundis, M. G. Campos, M.H. Farzaei, J. Xiao, Advances on natural polyphenols as anticancer agents for skin cancer, Pharmacol. Res. 151 (2020), 104584.
[33] M.G. Hertog, E.J. Feskens, P.C. Hollman, M.B. Katan, D. Kromhout, Dietary antioxidant flavonoids and risk of coronary heart disease: the Zutphen Elderly Study, Lancet 342 (1993) 1007–1011.
[34] S. Momtaz, A. Salek-Maghsoudi, A.H. Abdolghaffari, E. Jasemi, S. Rezazadeh, S. Hassani, M. Ziaee, M. Abdollahi, S. Behzad, S.M. Nabavi, Polyphenols targeting diabetes via the AMP-activated protein kinase pathway; future approach to drug discovery, Crit. Rev. Clin. Lab. Sci. 56 (7) (2019) 472–492.
[35] C. Giuliano, S. Cerri, F. Blandini, Potential therapeutic effects of polyphenols in Parkinson's disease: in vivo and in vitro pre-clinical studies, Neural Regener. Res. 16 (2021) 234–241.
[36] A. Singh, P. Tripathi, A.K. Yadawa, S. Singh, Promising polyphenols in Parkinson's disease therapeutics, Neurochem. Res. 45 (8) (2020) 1731–1745.
[37] A.C. Silveira, J.P. Dias, V.M. Santos, P.F. Oliveira, M.G. Alves, L. Rato, B.M. Silva, The action of polyphenols in diabetes mellitus and Alzheimer's disease: a common agent for overlapping pathologies, Curr. Neuropharmacol. 17 (7) (2019) 590–613.
[38] R. Sebori, A. Kuno, R. Hosoda, T. Hayashi, Y. Horio, Resveratrol decreases oxidative stress by restoring mitophagy and improves the pathophysiology of dystrophin-deficient mdx mice, Oxid. Med. Cell. Longev. 2018 (2018) 9179270.
[39] Y. Zhuang, H. Wu, X. Wang, J. He, S. He, Y. Yin, Resveratrol Attenuates Oxidative Stress-Induced Intestinal Barrier Injury through PI3K/Akt-Mediated Nrf2 Signaling Pathway, Oxid. Med. Cell. Longev. 2019 (2019) 7591840.
[40] S. Yilmaz, Effects of dietary caffeic acid supplement on antioxidant, immunological and liver gene expression responses, and resistance of Nile tilapia, Oreochromis niloticus to Aeromonas veronii Fish Shellfish Immunol. 86 (2019) 384–392.
[41] C. Magnani, V.L.B. Isaac, M.A. Correa, H.R.N. Salgado, Caffeic acid: a review of its potential use in medications and cosmetics, Anal. Methods. 6 (2014) 3203–3210.
[42] M. Battisti, S. De Martino, B. Miranda, Oxygen indicator films of acrylate photopolymers and TiO2 nanoparticles with tunable response times, Opt. Mater. . (2021). https://www.osapublishing.org/abstract.cfm?uri=ome-11-7-2244.
[43] P. Dardano, M. Battisti, I. Rea, L. Serpico, M. Terracciano, A. Cammarano, L. Nicolais, L. Stefano, Polymeric microneedle arrays: Versatile tools for an innovative approach to drug administration, Adv. Ther. 2 (2019) 1900036.
[44] P. Dardano, A. Caliò, J. Politi, I. Rea, I. Rendina, L. De Stefano, Optically monitored drug delivery patch based on porous silicon and polymer microneedles, Biomed. Opt. Express. 7 (2016) 1645–1655.
[45] Y.a. Gao, M. Hou, R. Yang, L. Zhang, Z. Xu, Y. Kang, P. Xue, Highly porous silk fibroin scaffold packed in pegda/sucrose microneedles for controllable transdermal drug delivery, Biomacromolecules 20 (3) (2019) 1334–1345.
[46] E.M. Boazak, V.K. Greene, D.T. Auguste, E. Lavik, The effect of heterobifunctional crosslinkers on HEMA hydrogel modulus and toughness, PLoS ONE 14 (5) (2019) e0215895.
[47] L. Serpico, M. De Nisco, F. Cermola, M. Manfra, S. Pedatella, Stereoselective synthesis of selenium-containing glycoconjugates via the mitsunobu reaction, Molecules 26 (9) (2021) 2541.
[48] T. Shimamura, Y. Sumikura, T. Yamazaki, A. Tada, Applicability of the DPPH assay for evaluating the antioxidant capacity of food additives–inter-laboratory evaluation study–, Analytical. (2014). https://www.jstage.jst.go.jp/article/analsci/30/7/30_717/_article/-char/ja/.
[49] P.L. Ritger, N.A. Peppas, A simple equation for description of solute release II. Fickian and anomalous release from swellable devices, J. Control. Release 5 (1987) 37–42, https://doi.org/10.1016/0168-3659(87)90035-6.
[50] C.S. Brazel, N.A. Peppas, Mechanisms of solute and drug transport in relaxing, swellable, hydrophilic glassy polymers, Polymer 40 (12) (1999) 3383–3398.
[51] Y. Fu, W.J. Kao, Drug release kinetics and transport mechanisms from semi-interpenetrating networks of gelatin and poly(ethylene glycol) diacrylate, Pharm. Res. 26 (9) (2009) 2115–2124.
[52] M.S. Blois, Antioxidant determinations by the use of a stable free radical, Nature 181 (4617) (1958) 1199–1200.
[53] I.F.F. Benzie, J.J. Strain, The Ferric Reducing Ability of Plasma (FRAP) as a Measure of "Antioxidant Power": The FRAP Assay, Anal. Biochem. 239 (1) (1996) 70–76.
[54] K.A. Wojtunik-Kulesza, Approach to optimization of FRAP methodology for studies based on selected monoterpenes, Molecules 25 (22) (2020) 5267.
[55] J.A. Vignoli, D.G. Bassoli, M.T. Benassi, Antioxidant activity, polyphenols, caffeine and melanoidins in soluble coffee: The influence of processing conditions and raw material, Food Chem. 124 (2011) 863–868.
[56] D. Villaño, M.S. Fernández-Pachón, M.L. Moyá, A.M. Troncoso, M.C. García-Parrilla, Radical scavenging ability of polyphenolic compounds towards DPPH free radical, Talanta 71 (1) (2007) 230–235.
[57] S. Zheng, I.A. Ashcroft, A depth sensing indentation study of the hardness and modulus of adhesives, Int. J. Adhes. Adhes. 25 (1) (2005) 67–76.
[58] R.W. Korsmeyer, N.A. Peppas, Solute and penetrant diffusion in swellable polymers. III. Drug release from glassy poly(HEMA-co-NVP) copolymers, J. Control. Release. 1 (2) (1984) 89–98.